Journal of Alloys and Compounds 493 (2010) 630–635

Contents lists available at ScienceDirect

Journal of Alloys and Compounds

journal homepage: www.elsevier.com/locate/jallcom

Effect of Zr^{4+} doping on the stabilization of ZnCo-mixed oxide spinel system and its catalytic activity towards N_2O decomposition

S.N. Basahel [a], I.H. Abd El-Maksod [a], B.M. Abu-Zied [b], M. Mokhtar [a,*]

[a] Chemistry Department, Faculty of Science, King Abdulaziz University, Jeddah 21569, Saudi Arabia
[b] Chemistry Department, Faculty of Science, Assiut University, Assiut 71516, Egypt

ARTICLE INFO

Article history:
Received 16 November 2009
Received in revised form
18 December 2009
Accepted 26 December 2009
Available online 4 January 2010

Keywords:
Spinel
Doping
$ZnCo_2O_4$
Activation energy
ESR
N_2O decomposition

ABSTRACT

Cobalt–zinc hydroxycarbonate precursor with nominal Co/Zn atomic ratio of 2 and 0.05–0.15 mol% ZrO_2-doped precursors have been synthesized from their metal nitrate and sodium carbonate by coprecipitation route. $ZnCo_2O_4$ spinel oxide was formed during the precipitation process as complemented by FTIR. Decomposition of the Co/Zn precursor at 350 °C resulted in the formation of $ZnCo_2O_4$ as evidenced by XRD technique. Zr^{4+}-doped samples stabilized the $ZnCo_2O_4$ phase and suppressed the formation of ZnO phase at 550 and 750 °C. The highest surface areas (S_{BET}) were attained for the samples doped with 0.15 mol% ZrO_2. Activation energy of sintering derived from XRD and S_{BET} data was directly proportional to the dopant concentration. ESR results revealed that the addition of increased amounts of Zr^{4+} enhances the formation of Co^{2+} ions. The activity of the 350 and 750 °C calcined catalysts was tested for N_2O direct decomposition. The observed activities were related to the presence of Co^{2+}–Co^{3+} ion pairs which were enhanced by the addition of Zr^{4+} ions.

© 2009 Elsevier B.V. All rights reserved.

1. Introduction

Nitrous oxide (N_2O) contributes significantly to the destruction of ozone in the stratosphere and is considered as a strong greenhouse gas [1,2]. The atmospheric lifetime of nitrous oxide is about 120 years and its present concentration is 311 ppb, whereas its Global worming potential is 310 times higher than that of CO_2 [3]. Under the Kyoto Protocol of the United Nations Convention on Climate Change, industrialized countries agreed to reduce their collective green house gas emissions by about 5% from the level in 1990 [4]. Several catalysts have been tested for the catalytic decomposition of nitrous oxide gas to its elements, i.e. N_2 and O_2 [5–14]. Recently, spinel-type oxides have been a subject of increasing applied research [15–21] in addition to be used as efficient catalysts [22–24]. The chemical formula of the spinel structure generally is AB_2O_4 in which A ions are generally divalent cations occupying tetrahedral sites and B ions are trivalent cations in octahedral sites [25]. Cobalt containing spinels, was shown to be superior to other transition metal spinels towards the N_2O decomposition in presence or in absence of oxygen [11,25–29].

The solid-state reaction of the parent metal oxides considered to be the most general method for preparing oxide spinels. However, for attaining complete reaction, a temperature of about 1000 °C (or higher) has to be maintained for several days [30]. The disadvantages of solid-state routes, such as inhomogeneity, lack of stoichiometry control, and larger particle size are avoided when the material is synthesized using a solution-based method. Coprecipitation of mixed metal salts with alkaline carbonates at low super-saturation and constant pH provide a single phase mixed metal carbonates and hydroxycarbonates which form high surface area metal oxides by calcination [31]. Among the transition metals (viz. Mn, Co, Cr, Fe and Ni)-doped ZrO_2 (cubic) catalysts, cobalt-doped ZrO_2 showed the highest activity for the toluene combustion [32]. Zirconium oxide promoted the selective reforming of methanol reaction and slightly reduced the concentration of CO when it is incorporated in $CuO/ZnO/Al_2O_3$ system [33]. The $CuO/ZnO/ZrO_2/Al_2O_3$ catalysts were reported as good candidates for the selective reforming of methanol, as determined by comparison with the commercial catalyst G66B [33]. In the present work, incorporating ZrO_2 as a dopant into the cobalt/zinc spinel oxides prepared via thermal decomposition of co-precipitated hydroxy carbonate salts will be investigated. To the author's knowledge the cobalt/zinc doped with ZrO_2 catalyst system has not yet used as a catalyst in N_2O decomposition. An intensive study of the structural and catalytic N_2O decomposition over ZrO_2-doped cobalt/zinc-mixed oxide catalysts will be carried out in this research.

* Corresponding author. Tel.: +966 500558045; fax: +966 2 6952292.
E-mail addresses: mmokhtar2000@yahoo.com, mmoustafa@kau.edu.sa (M. Mokhtar).

0925-8388/$ – see front matter © 2009 Elsevier B.V. All rights reserved.
doi:10.1016/j.jallcom.2009.12.169

2. Experimental

2.1. Catalysts preparation

A series of un-doped and ZrO_2-doped Zn–Co oxides were prepared by coprecipitation method using two solutions namely (A) and (B). Solution (A) contained the desired amount of metal nitrates and solution (B) consisted of precipitating agents (1 M Na_2CO_3). The two solutions were added simultaneously, while the pH was maintained at ca. 7 under vigorous stirring at 60 °C for 5 h. Finally all samples were washed by re-deposition in distilled water under gentle stirring and filtration. This washing/filtration step was repeated 5 times till the precipitate was free from sodium ions as confirmed from ICP analyses. The precipitate then dried at 80 °C for 16 h and calcined in air at 350, 550 and 750 °C. The catalysts obtained were denoted $Zn_1Co_2Zr_z$, where z refers to Zr mol%.

2.2. Techniques

X-ray powder diffraction studies were conducted to all the prepared solid samples by means of Bruker diffractometer (Bruker D8 advance target). The patterns were run with Cu Kα with secondly monochromator (λ = 1.5405 Å) at 40 kV and 40 mA. The crystallite size of $ZnCo_2O_4$ phase was calculated using Scherrer equation:

$$D = B\frac{\lambda}{\beta_{1/2}}\cos\theta \quad (1)$$

where D is the average crystallite size of the phase under investigation, B the Scherrer constant (0.89), λ the wavelength of the X-ray beam used (1.54056 Å), $\beta_{1/2}$ the full width at half maximum (FWHM) of diffraction peak and θ is the diffraction angle. The patterns obtained were matched with the standard data for the purpose of phase identification. FTIR spectra were recorded in the range 400–4000 cm^{-1} on PerkinElmer Spectrum 100 FTIR spectrometer. The infrared spectra were recorded at room temperature for the prepared products using KBr disk technique. The resulting FTIR spectral pattern was then analyzed and matched with known signatures of identified materials in the FTIR library. The specific surface area of the prepared samples were determined from nitrogen adsorption/desorption isotherms measurements at −196 °C using a model NOVA 3200e automated gas sorption system (Quantachrome, U.S.A.). Prior to measurement, each sample was degassed for 6 h at 150 °C. The specific surface area, S_{BET}, was calculated by applying the Brunauer–Emmett–Teller (BET) equation [34]. ESR spectra of different solids were measured using (Brucker Elexsys 500) operated at X-band frequency. The following parameters are generalized to all samples otherwise mentioned in the text. Microwave frequency, 9.73 GHz; receiver gain, 20; sweep width, 6000; center at 3480; and microwave power 0.00202637 W.

2.3. Catalyst activity measurements

The catalytic reaction was carried out in a fixed-bed quartz flow reactor, containing 100 mg of the catalyst in all the experiments. The temperature in the reactor was measured using a thermocouple adjacent to the catalyst bed. Prior to each experiment the catalyst was treated in N_2 at 350 and 500 °C, for 1 h, for the catalysts calcined at 350 and 750 °C, respectively. The temperature was measured by a K-type thermocouple inserted in the catalyst bed and was controlled by a Cole–Parmer temperature controller (model *Digi-Sense* 89000-00). N_2O (500 ppm) was added with the aid of thermal mass flow controllers (AALBORG, DFC2600) using N_2 as a balance gas, the volume flow rate was 200 cm^3/min (NTP). The exit concentrations were monitored by means of a magnetic oxygen analyzer (ABB, AO2020-Magnos 106) and non-dispersive infrared analyzer for the components N_2O, NO (ABB, AO2020-Uras 14). Preliminary experiments for the decomposition of nitrous oxide over all the catalysts showed the absence of NO in the exit gas.

3. Results and discussion

3.1. Powder X-ray diffraction (PXRD)

X-ray diffraction patterns of calcined $Zn_1Co_2Zr_{0.0–0.15}$ system is shown in Fig. 1. The diffraction patterns, of the calcined product at 350 °C, are consistent with $ZnCo_2O_4$ phase (Ref. pattern 81-2299, JCPDS). The percentage abundance of $ZnCo_2O_4$ phase was correlated to the relative intensity of the diffraction patterns. Addition of 0.05 mol% ZrO_2 resulted in a slight increase in the intensity of the $ZnCo_2O_4$ reflections. Moreover, the 0.15 mol% ZrO_2 doping resulted in a pronounced increase in the relative intensity of all the diffraction pattern of $ZnCo_2O_4$ phase. Un-doped samples calcined at 550 and 750 °C showed the formation of impurities peaks of zincite (ZnO) [JCPDS 36-1451] together with the $ZnCo_2O_4$ phase (Fig. 1). The addition of smallest amount of ZrO_2 suppresses the zincite phase patterns and enhances the formation of single spinel structure. The crystal structure of the investigated spinel was tetragonal body centered with 141/acd point group (Table 1). From the results of the XRD, the increase in the lattice parameters, a and c, for the doped samples was found. Increasing Zr^{4+} doping from 0.05 to 0.15 mol% led to a change in lattice parameters for the investigated samples calcined at different temperatures. However, the Zr^{4+} doping does not give rise to a distortion of the crystalline structure. The change in the lattice parameters could be attributed to the larger ion size of Zr^{4+} (0.86 Å) compared to that of Co^{3+} (0.685 Å).

The calculated crystallite size values, using Scherrer equation, were increased with the increase of calcination temperature from 350 to 750 °C for all the investigated solids. The computed values of the particle size of $ZnCo_2O_4$ in un-doped and doped solids preheated at 350–750 °C enabled the calculation of the activation

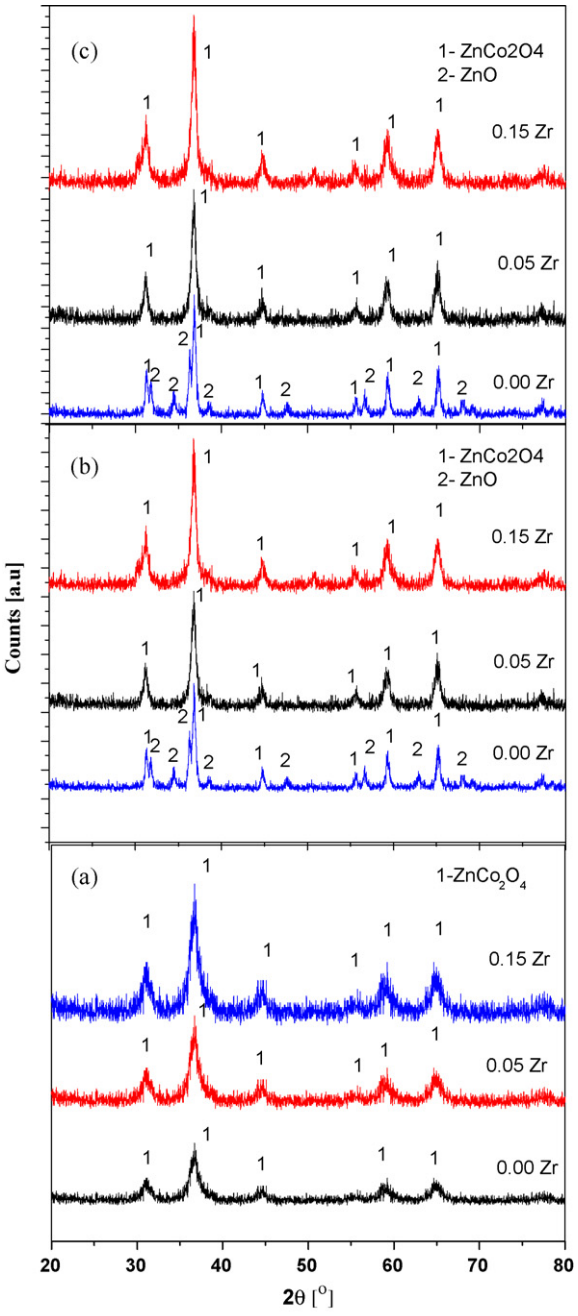

Fig. 1. XRD patterns of $Zn_1Co_2Zr_{0.0–0.15}$ calcined at different temperatures obtained for the catalysts being calcined at 350 (a), 550 (b) and 750 °C (c).

Table 1
XRD data obtained for $ZnCo_2O_4$ patterns of calcined samples at different temperatures.

Catalyst	Phases	Cryst. size (nm)	Crystal system	Lattice parameters		E_s (kJ/mol)
				a	c	
$Zn_1Co_2Zr_{0.00}$ 350 °C	$ZnCo_2O_4$	8	Tetragonal body centered I41/acd	10	9.01	20.0
$Zn_1Co_2Zr_{0.00}$ 550 °C	ZnO, $ZnCo_2O_4$	16	Tetragonal body centered I41/acd	5.71	6.28	
$Zn_1Co_2Zr_{0.00}$ 750 °C	ZnO, $ZnCo_2O_4$	38	Tetragonal body centered I41/acd	9.0	15.2	
$Zn_1Co_2Zr_{0.05}$ 350 °C	$ZnCo_2O_4$	11	Tetragonal body centered I41/acd	9.8	9.01	21.14
$Zn_1Co_2Zr_{0.05}$ 550 °C	$ZnCo_2O_4$	28	Tetragonal body centered I41/acd	6.1	17.3	
$Zn_1Co_2Zr_{0.05}$ 750 °C	$ZnCo_2O_4$	56	Tetragonal body centered I41/acd	8.1	6.1	
$Zn_1Co_2Zr_{0.15}$ 350 °C	$ZnCo_2O_4$	10	Tetragonal body centered I41/acd	11.0	8.0	25.3
$Zn_1Co_2Zr_{0.15}$ 550 °C	$ZnCo_2O_4$	33	Tetragonal body centered I41/acd	11.8	4.9	
$Zn_1Co_2Zr_{0.15}$ 750 °C	$ZnCo_2O_4$	68	Tetragonal body centered I41/acd	13.0	8.0	

energy of sintering (E_S) of zinc cobaltite phase using Arrhenius equation:

$$D = A\exp^{(-E_S/RT)} \quad (2)$$

where D is the crystallite size of $ZnCo_2O_4$ preheated at temperature T, A the frequency factor of Arrhenius equation and E_s is the activation energy of sintering process of Zn–Co oxide spinel. By plotting $\ln D$ vs. $1/T$ a straight line is obtained whose slope and intercept permitted the calculation of E_s and $\ln A$. The Arrhenius plots in the range of 350–750 °C for un-doped and those doped with different mol% of ZrO_2 are given in Fig. 2. The computed E_s values were 20, 21.14 and 25.3 kJ mol^{-1} for un-doped and those doped with 0.05 and 0.15 mol% ZrO_2, respectively. These results suggested that ZrO_2 doping retarded the sintering due to grain growth or particle adhesion of $ZnCo_2O_4$ crystallites.

3.2. FTIR spectra

The FTIR spectra of ZnCo-hydroxycarbonate precursor are given in Fig. 3a. It is clear that five sharp absorption bands with maxima at 500–590, 600–790,1250–1500, 1500–1750 cm^{-1} and one broad band 3300–3600 cm^{-1}. Characteristic vibrational modes of the carbonate group at 1402, 1488 and 1653 cm^{-1} were in accordance with literature data [35]. Broad intense band at $\nu = 3358$ cm^{-1} due to the OH^- stretching mode and water molecules were observed [36]. The intensity of such broad band decreases up on calcination of the catalyst precursors at different calcination temperatures. The two absorption bands with maxima at 678 and 578 cm^{-1} were observed in the IR spectra of perfect $ZnCo_2O_4$ spinel [37,38]. Accordingly, the spinel-like structure is formed immediately after the precipitation prior to calcination of the samples. The splitting and asymmetry of the spinel absorption bands are attributed to the presence of different cations located at the same crystallographic positions [39]. Thus, the data obtained could be attributed to the presence

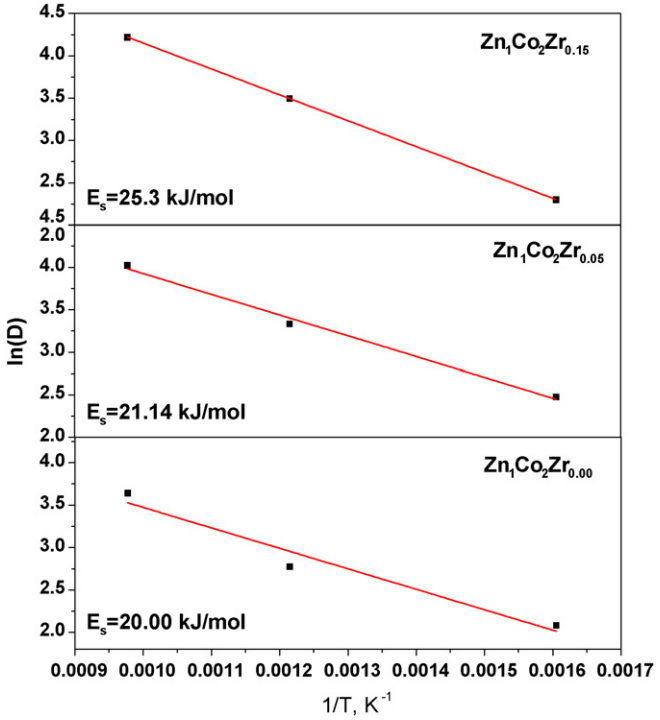

Fig. 2. Arrhenius plots of activation energy of sintering for different investigated systems calculated from XRD data.

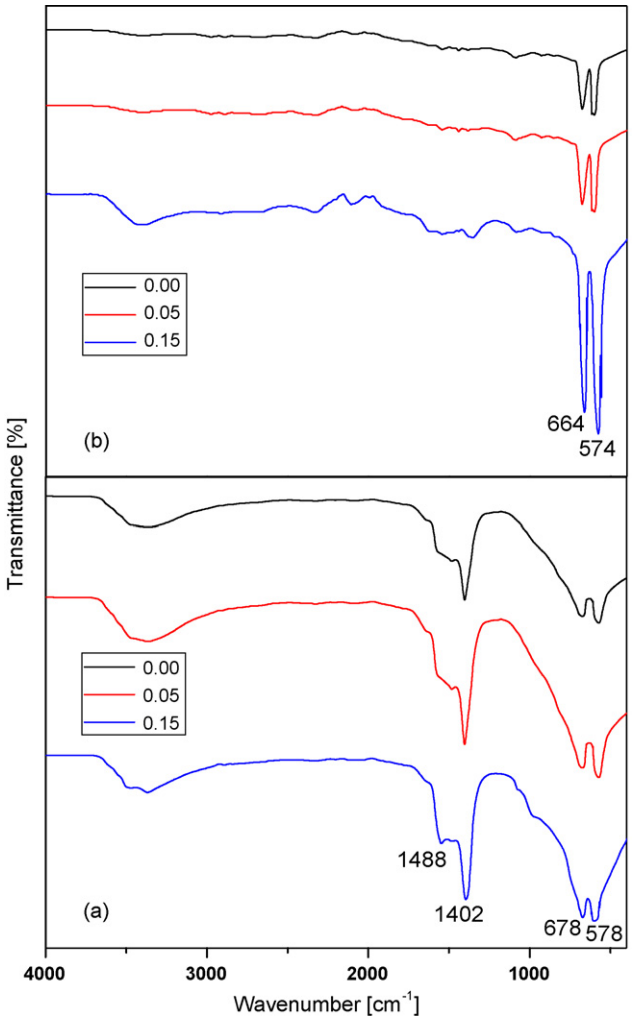

Fig. 3. FTIR of $Zn_1Co_2Zr_{0.0–0.15}$ obtained for the precursors (a) and the 350 °C calcined catalysts (b).

Table 2
BET-surface area and activation energy of sintering (E_s) of different investigated samples.

Catalyst	Phases	S_{BET} (m^2/g)	E_s (kJ/mol)
$Zn_1Co_2Zr_{0.00}$ 350 °C	$ZnCo_2O_4$	55	13.40
$Zn_1Co_2Zr_{0.00}$ 550 °C	$ZnCo_2O_4$, ZnO	33	
$Zn_1Co_2Zr_{0.00}$ 750 °C	$ZnCo_2O_4$, ZnO	20	
$Zn_1Co_2Zr_{0.05}$ 350 °C	$ZnCo_2O_4$	85	18.38
$Zn_1Co_2Zr_{0.05}$ 550 °C	$ZnCo_2O_4$	50	
$Zn_1Co_2Zr_{0.05}$ 750 °C	$ZnCo_2O_4$	20	
$Zn_1Co_2Zr_{0.15}$ 350 °C	$ZnCo_2O_4$	99	19.17
$Zn_1Co_2Zr_{0.15}$ 550 °C	$ZnCo_2O_4$	72	
$Zn_1Co_2Zr_{0.15}$ 750 °C	$ZnCo_2O_4$	21	

of both Co and Zn cations in octahedral as well as in tetrahedral positions of the spinel structure. The intensities of $ZnCo_2O_4$ spinel bands increase as the ZrO_2 mol% increase. The addition of 0.15 ZrO_2 resulted in a pronounced increase in the intensity of the spinel bands. The increase in intensity of FTIR bands could clarify the role of Zr^{4+} towards the stabilization of $ZnCo_2O_4$ phase detected in XRD patterns.

FTIR spectra of the calcined catalyst precursors at 350 °C are given in Fig. 3b. It is obvious that, the intensities of the two spinel bands increase with temperature increasing to 350 °C. Moreover, the carbonate and the OH^- bands were greatly diminished. The intensity of $ZnCo_2O_4$ bands was in accordance with the increase in ZrO_2 content. These results complement the appearance of single $ZnCo_2O_4$ phase for the solids calcined at 350 °C as confirmed by XRD results.

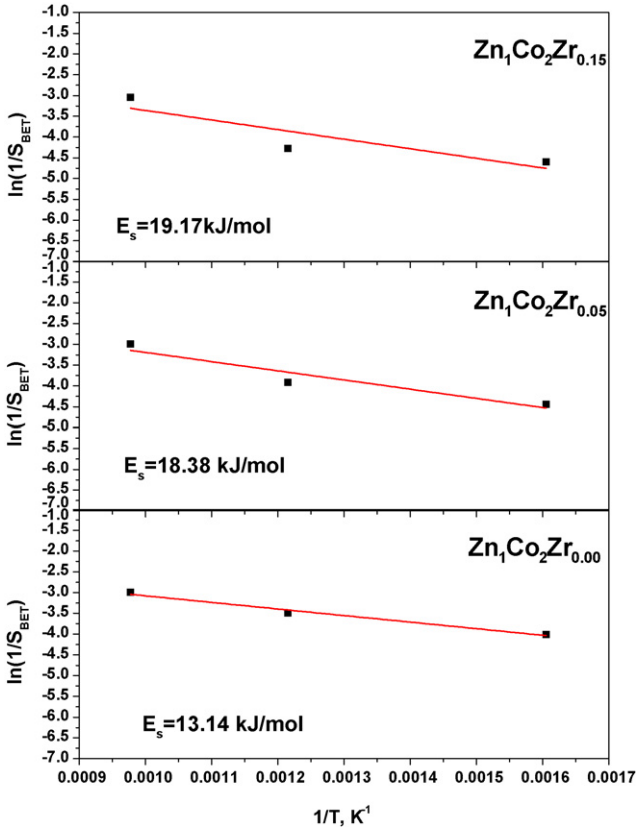

Fig. 4. Arrhenius plots of activation energy of sintering for different investigated systems calculated from S_{BET} data.

3.3. N_2 adsorption

The specific surface areas (S_{BET}) of all the investigated solids were measured by adsorption of N_2 at −196 °C. The S_{BET} values obtained are cited in Table 2. It is shown from these data that the surface area of $ZnCo_2O_4$ spinel is relatively large in comparing with those prepared in literature using the coprecipitation method [40]. The addition of small amount of ZrO_2 dopant resulted in a pronounced increase in the S_{BET} values except for the samples calcined at 750 °C. In addition to that the specific surface areas of all the investigated samples were decreased monotonically with the elevation of the calcination temperature from 350 to 750 °C. The activation energy of sintering (E_s) was calculated from the relation between $\ln(1/S_{BET})$ vs. $1/T$ using Arrhenius equation [41]. The Arrhenius plots are presented in Fig. 4 and the data obtained were cited in Table 2. E_s values were increased upon increasing the amount of ZrO_2 content. This increase in the E_s values indicates the retardation of ZrO_2 to the collapse in the pore structure, i.e. hindering the sintering process. The obtained values of E_s, are in agreement with the E_s values obtained from XRD data. E_s values show that the sintering of the investigated samples took place via collapse of the pore structure due to the grain growth mechanism [36].

3.4. ESR spectra

Fig. 5 displays the ESR spectra obtained for the different doped and un-doped samples calcined at 350 and 750 °C. It is clear from this figure that the ESR spectra of un-doped samples showed very

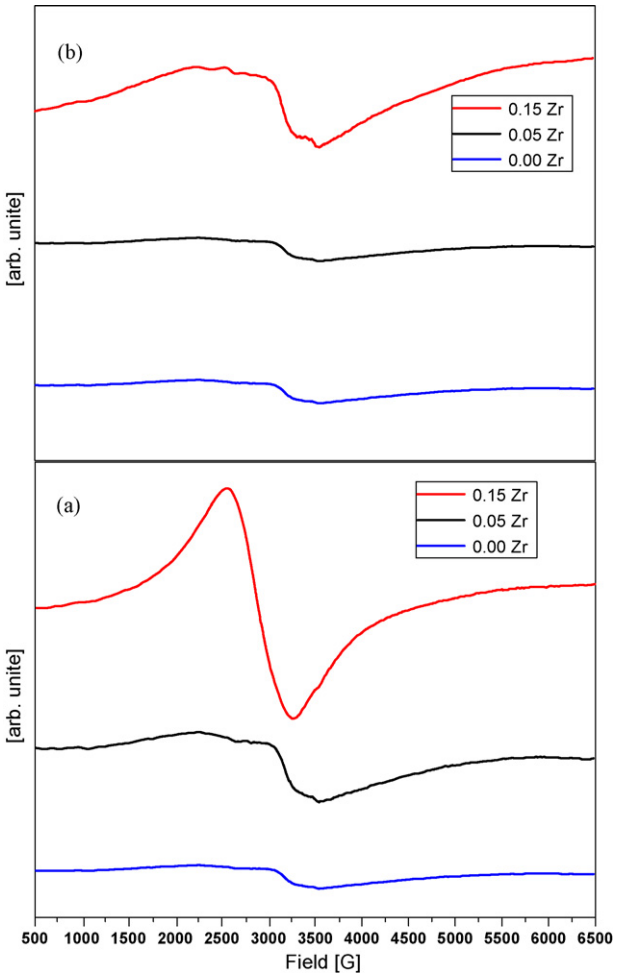

Fig. 5. ESR spectra of $Zn_1Co_2Zr_{0.0-0.15}$ system calcined at 350 (a) and 750 °C (b).

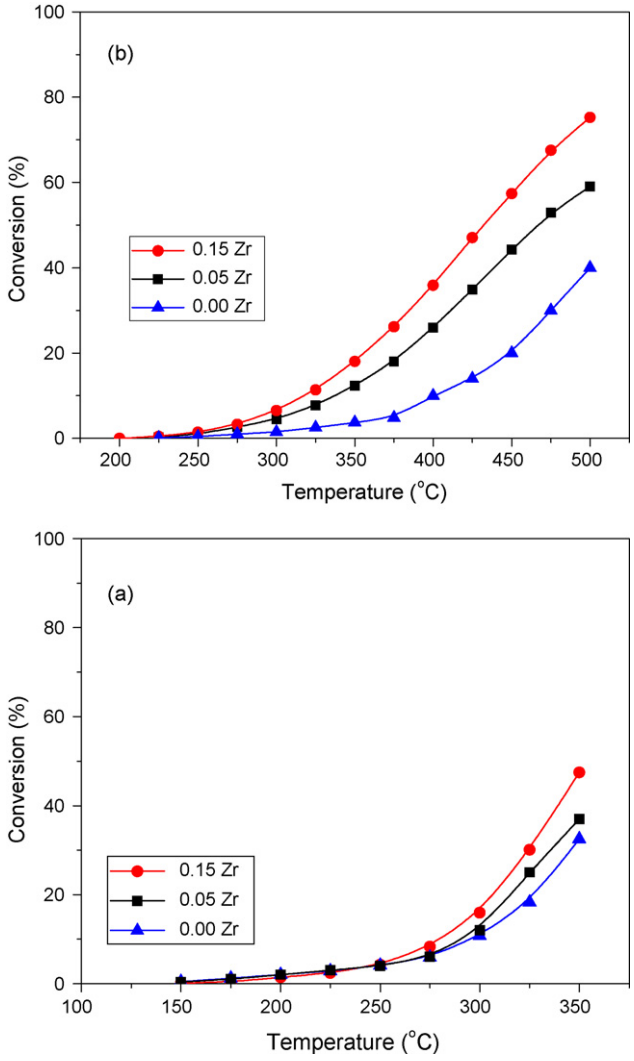

Fig. 6. N_2O decomposition over $Zn_1Co_2Zr_x$ catalysts being calcined at 350 (a) and 750 °C (b).

low intensities of ESR signal regardless the calcination temperature. This suggests that the cobalt in the un-doped samples present as Co^{3+}, since Co^{2+} is responsible for the appearance of ESR signals [42]. In other words, cobalt exists mainly in the B site of the $ZnCo_2O_4$ spinel. On the other hand, introducing Zr^{4+} as a dopant (0.05 and 0.15 mol%) is accompanied by a remarkable increase in ESR signal intensity. This suggests that Zr^{4+} stabilizes certain species that contains Co^{2+}. Although the XRD diffractograms did not recognize any other species rather than $ZnCo_2O_4$ and ZnO, the presence of Co^{2+} could be attributed to the migration of cobalt in the spinel structure replacing some of Zn^{2+} to form $CoCo_2O_4$. The XRD peaks of this phase are nearly the same for $ZnCo_2O_4$ which explain that XRD could not recognize the differences between these phases [31]. Moreover, a decrease in ESR signal was observed in all samples upon increasing the calcination temperature from 350 to 750 °C. This decrease in signal intensities reflects a decrease in Co^{2+} with the temperature rise. However, the samples containing Zr^{4+} still exhibit higher ESR signal.

3.5. N_2O decomposition

Fig. 6 shows the temperature dependence of N_2O conversion over the 350 and 750 °C calcined catalysts. It is evident that N_2O decomposition increases with raising the temperature over all the catalysts. The onset of the reaction starts at 175 °C for the 350 °C calcined catalysts and at 250 °C for the 750 °C calcined ones. This indicates a higher activity of the lower temperature calcined catalysts. In this respect, 47 and 18 conversion % at 350 °C reactor temperature over the $Zn_1Co_2Zr_{0.15}$ calcined at 350 and 750 °C, respectively. Within the same series the activity increases with increasing the Zr content in catalyst.

The suggested mechanism for N_2O decomposition over cobalt containing spinel oxides includes the following steps [29,43,44]:

$$N_2O_{(g)} + Co^{2+} \rightarrow N_2O_{(ads.)}{}^{-}\cdots Co^{3+} \quad (3)$$

$$N_2O_{(ads.)}{}^{-}\cdots Co^{3+} \rightarrow N_{2(g)} + O_{(ads.)}{}^{-}\cdots Co^{3+} \quad (4)$$

$$O_{(ads.)}{}^{-}\cdots Co^{3+} \rightarrow \frac{1}{2}O_{2(g)} + Co^{2+} \quad (5)$$

In this mechanism, the simultaneous coexistence of +2 and +3 oxidation states would ease the recovering process, thus enhancing the N_2O decomposition activity. From the combination of the data presented in Figs. 5 and 6 two points could be raised: (i) the higher activity of the zirconia containing catalysts could be related to the stabilization role of zirconia to the Co^{2+} ions, in other words to the increased numbers of Co^{2+}–Co^{3+} redox couple, and (ii) the lower activity of the 750 °C calcined catalysts compared to the relevant catalysts calcined at 350 °C could be understood in terms of the observed decrease in the Co^{2+} ions as well as the decrease in the obtained S_{BET} values (Table 2) accompanying the increase in the calcination temperature.

4. Conclusions

Controlled co-precipitation considered as an effective route in the formation of $ZnCo_2O_4$ spinel immediately before calcination at even low temperature. ZrO_2 doping enhances the stabilization of $ZnCo_2O_4$ spinel structure even at high calcination temperature (750 °C). ZrO_2 doping resists the sintering process as evidenced by E_s values and increases the S_{BET} of the doped samples calcined at 350 and 550 °C. The concentration of Co^{2+} species was enhanced by addition of Zr^{4+} to the Co/Zn system calcined at 350 and 750 °C calcined catalysts. Such effect is reflected in a higher N_2O decomposition activity of the zirconia containing catalysts.

Acknowledgements

We are grateful to the Deanship of Scientific Research at King Abdulaziz University for supporting the present work. We would like to gratefully acknowledge the Deutscher Akademischer Austausch Dienst (DAAD) for the granting of the gas analyzers used in the N_2O decomposition measurements.

References

[1] J.C. Kramlich, W.P. Linak, Prog. Energy Combust. Sci. 20 (1994) 149.
[2] M.A. Wojtowicz, J.R. Pels, J.A. Moulijn, Fuel Proc. Technol. 34 (1993) 1.
[3] J. Pérez-Ramírez, Appl. Catal. B 70 (2007) 31–35.
[4] Available from: http://en.wikipedia.org/wiki/Kyoto_Protocol.
[5] B.M. Abu-Zied, Appl. Catal. A 334 (2008) 234.
[6] B.M. Abu-Zied, W. Schwieger, A. Unger, Appl. Catal. B 84 (2008) 277.
[7] B.M. Abu-Zied, W. Schwieger, Appl. Catal. B 85 (2009) 120.
[8] J. Pérez-Ramírez, F. Kapteijn, G. Mul, J.A. Moulijn, Chem. Commun. (2001) 693.
[9] F. Kapteijn, J. Rodriguez-Mirasol, J.A. Moulijn, Appl. Catal. B 9 (1996) 25.
[10] P. Granger, P. Esteves, S. Kieger, L. Navascues, G. Leclercq, Appl. Catal. B 26 (2006) 236.
[11] N. Russo, D. Fino, G. Saracco, V. Specchia, Catal. Today 119 (2007) 228.
[12] A. Miguel, P. Javier, Appl. Catal. B 77 (2008) 248.
[13] T. Turek, Catal. Today 105 (2005) 275.
[14] R. Sundararajan, V. Srinivasan, Appl. Catal. 73 (1991) 165.
[15] H.G. El-Shobaky, Appl. Catal. A 278 (2004) 1.
[16] T. Kawano, J. Takahashi, T. Okutani, T. Yamada, H. Yamane, J. Alloys Compd. 468 (2009) 447.

[17] S.M. Yunus, H. Yamauchi, A.K.M. Zakaria, N. Igawa, A. Hoshikawa, Y. Haga, Y. Ishii, J. Alloys Compd. 455 (2008) 98.
[18] M. Obata, H. Hayashi, A. Kishimoto, J. Alloys Compd. 471 (2009) L32.
[19] S.S. Ata-Allah, M. Kaiser, J. Alloys Compd. 471 (2009) 303.
[20] R.N. Bhowmik, R. Ranganathan, B. Ghosh, S. Kumar, S. Chattopadhyay, J. Alloys Compd. 456 (2008) 348.
[21] S.M. Yunus, H. Yamauchi, A.K.M. Zakaria, N. Igawa, A. Hoshikawa, Y. Ishii, J. Alloys Compd. 454 (2008) 10.
[22] Y. Liang, R. Tong, W. Xiaolai, J. Dong, S. Jishuan, Appl. Catal. B 45 (2003) 85.
[23] Y. Wang, J. Zhang, J. Zhu, J. Yin, H. Wang, Energy Conv. Manage. 50 (2009) 1304.
[24] M.J. Pollard, B.A. Weinstock, T.E. Bitterwolf, P.R. Griffiths, A.P. Newbery, J.B. Paine, J. Catal. 254 (2008) 218–225.
[25] P. Stelmachowski, G. Maniak, A. Kotarba, Z. Sojka, Catal. Commun. 10 (2009) 1062.
[26] Q. Shen, L. Li, J. Li, H. Tian, Z. Hao, J. Hazard. Mater. 163 (2009) 1332.
[27] K. Papadatos, K.A. Shelstad, J. Catal. 28 (1973) 116.
[28] F. Song, L. Huang, D. Chen, W. Tang, Mater. Lett. 62 (2008) 543.
[29] B.M. Abu-Zied, S.A. Soliman, Catal. Lett. 132 (2009) 299.
[30] C.O. Aréan, M.P. Mentruit, A.J.L. López, J.B. Parra, Phys. Eng. Aspects 180 (2001) 253.
[31] T. Baird, K.C. Campbell, P.J. Holliman, R.W. Hoyle, D. Stirling, B.P. Williams, M. Morrisc, J. Mater. Chem. 7 (1997) 319.
[32] V.R. Choudhary, G.M. Deshmukh, S.G. Pataskar, Catal. Commun. 5 (2004) 115.
[33] G. Huang, B. Liaw, C. Jhang, Y. Chen, Appl. Catal. A 358 (2009) 7.
[34] S. Brunauer, P.H. Emmett, E. Teller, J. Am. Chem. Soc. 60 (1938) 309.
[35] J. Preudhomme, P. Tarte, Spectrochim. Acta 27 (1971) 1817.
[36] M. Mokhtar, M.W. Kadi, Mater. Technol. 24 (2009) 100.
[37] V. Rives, S. Kannan, J. Mater. Chem. 10 (2000) 489.
[38] G.N. Kustova, E.B. Burgina, G.G. Volkova, T.M. Yurieva, L.M. Plyasova, J. Mol. Catal. A 158 (2000) 293.
[39] S.Z. Hafner, Krist 119 (1961) 331.
[40] M. Santiago, M.A.G. Hevia, J. Pérez-Ramírez, Appl. Catal. B 90 (2009) 83.
[41] Th. El-Nabarawy, M. Mokhtar, G.A. El-Shobaky, Ads. Sci. Technol. 12 (1995) 27.
[42] P. Cossee, J. Inorg. Nucl. Chem. 8 (1958) 483.
[43] U. Chellam, Z.P. Xu, H.C. Zeng, Chem. Mater. 12 (2000) 650–658.
[44] H.C. Zeng, J. Lin, W.K. Teo, J.C. Wu, K.L. Tan, J. Mater. Res. 10 (1995) 545–552.